ISSN1346－7832

独立行政法人港湾空港技術研究所

港湾空港技術研究所報告

REPORT OF THE PORT AND AIRPORT RESEARCH INSTITUTE

VOL.43 NO.4 December 2004

NAGASE, YOKOSUKA, JAPAN

INDEPENDENT ADMINISTRATIVE INSTITUTION,
PORT AND AIRPORT RESEARCH INSTITUTE

港湾空港技術研究所報告（REPORT OF PARI）
第 43 巻　第 4 号（Vol. 43, No. 4），　2004年12月（December 2004）

目　　次（CONTENTS）

REPORT OF THE PORT AND
AIRPORT RESEARCH INSTITUTE
Vol.43, No.4 (Dec., 2004)

Modeling wetting and drying scheme based on an extended logarithmic law for a three-dimensional sigma-coordinate coastal ocean model

Yusuke UCHIYAMA*

Synopsis

A wetting and drying scheme (WDS) is developed to incorporate into a three-dimensional sigma-coordinate coastal ocean model (POM; Blumberg and Mellor, 1983) with proposing an extended logarithmic profile within and above bed boundary layers to accurately simulate 3D hydrodynamics in extremely shallow coastal seas. While the WDS is simplistically formulated, it can selectively retain the computational robustness and water mass conservation in the domain. The developed model, WD-POM, is verified to have a good agreement with the analytical solution for non-linear long-waves propagating on a sloping beach proposed by Carrier and Greenspan (1958). WD-POM is also applied to a tidal simulation in San Francisco Bay, California, USA, which is encompassed by huge intertidal areas. The model-generated surface elevations and tidal currents are compared to the observed data-set by NOS-NOAA (2003) and demonstrate that WD-POM is capable of precisely reproducing the estuarine intertidal hydrodynamics in San Francisco Bay.

The influence of intertidal topographies on estuarine hydrodynamics is next examined, by comparing between the simulated result with WDS and that without WDS. The wetting and drying process is represented to significantly alter development of tidal waves and a current field in San Francisco Bay. The intertidal sloping bathymetry appears to enhance refraction and shoaling of tidal waves propagating anticlockwise as Kelvin waves. The intertidal effects are evidently exhibited to modify the amplitude and phase speed of the tidal waves, and to shift the current direction to be shore-normal.

Key Words: wetting and drying, intertidal flat, estuary, hydrodynamics, bed boundary layer

* Senior Researcher, Littoral Drift Division, Marine Environment and Engineering Department
3-1-1 Nagase, Yokosuka 239-0826, Japan
phone: +81-46-844-5045, facsimile: +81-46-841-9812, email: uchiyama@pari.go.jp

港湾空港技術研究所報告
第43巻第4号（2004.12）

拡張対数則を導入した干出・冠水スキームの開発と3次元σ座標海洋モデルへの適用

内山　雄介*

要　旨

3次元σ座標系海洋流動モデル（POM; Blumberg and Mellor, 1983）に適用可能な干出・冠水スキーム（WDS）を開発した．WDSでは，拡張対数則を新たに導入することにより，干出域を含む潮間帯において水深が極めて浅くなった場合でも底面境界層周辺の流速場を正確に再現することが可能となっている．このWDSはシンプルな形で定式化されているが，領域全体の質量保存と計算上のロバストネスを選択的に確保することができるようにモデリングされている．開発された3次元モデル（WD-POM）の再現性を確認するため，計算結果をCarrier and Greenspan（1958）による非線形長波の斜面遡上問題に対する理論解と比較したところ，両者は良好に一致した．次いで，広大な潮間帯を有する内湾海域である米国サンフランシスコ湾の潮流計算にWD-POMを適用したところ，モデルによる潮位変動と潮流速変動がNOS-NOAA（2003）による観測結果とほぼ完全に一致したことから，WD-POMが潮間帯を含む内湾域の流動を忠実に再現することが可能であることが確認された．

潮間帯の存在が内湾流動におよぼす影響を照査するため，サンフランシスコ湾の地形に対してWDSを適用した場合としない場合の計算を実施し，両者の結果を比較した．潮間帯の存在は湾内における潮汐波の伝播と沿岸部における潮汐残差流の形成に対して重大な影響を及ぼしていることが実証された．すなわち，ケルビン波として湾内を反時計回りに伝播する潮汐波は，潮間帯上の斜面を遡上する際に屈折変形を受けて等深線に垂直な流速成分を生じると同時に，浅水変形により潮位変動振幅が増大し，逆に底面摩擦の影響が相対的に大きくなるため潮汐波伝播の位相が遅れることなどが明らかとなった．

キーワード：冠水・干出，潮間帯干潟，内湾海域，流動，底面境界層

*　海洋・水工部　漂砂研究室　主任研究官
〒239-0826　神奈川県横須賀市長瀬3-1-1
電話：046-844-5045，FAX：046-841-9812，Eメール：uchiyama@pari.go.jp

CONTENTS

1. INTRODUCTION

Estuarine intertidal mudflats and salt marshes have been recognized to play a significant role in marine environment and aquatic ecosystems. Efforts have been made to investigate hydrodynamics and associated sediment transport as well as chemical substances attached to the sediment particles on intertidal areas (Kuwae *et al.*, 1998; Austen *et al.*, 1999; Van Der Lee, 2000; Le Hir, *et al.* 2000; Uchiyama *et al.*, 2001; Talke and Stacey, 2003). A key factor dominating intertidal hydrodynamics is a wetting and drying process as it affects suction of pore water in bed sediments influencing on sediment suspension, evaporation related to thermal and salinity environments of overlaying seawater, rapid movement of tidal currents resulting in formation of highly turbid "tidal bore" on the bed, and so on (Whitehouse *et al.*, 2000). These facts imply that it is important to resolve the vertical structure within and above the bed boundary layer in order to precisely assess intertidal environments including sediment suspension and deposition.

Numerical experiments have been frequently performed to investigate estuarine hydrodynamics and transport processes, whereas the wetting and drying process in intertidal areas is often neglected. A proper approach to replicate the flooding-draining processes, i.e., submergence at high water and emergence at low water, must thus be developed. In terms of mathematics, however, this seems intricate because the computational domain varies with time if intertidal process must be taken into account (Cheng *et al.*, 1993). Attempts have been made to solve this problem for the last two or three decades and two different approaches have been developed: a moving boundary method and a wet-dry point treatment method. In the moving boundary method, the computational domain, or the model grid system, is reconfigured for each time step according to the boundary defined by a zero total depth and a zero normal transport at an interface between land and water (Lynch and Grey, 1980; Siden and Lynch, 1988; Austria and Aldama, 1990; Shi, 1995; Hervouet and Van Haren, 1996; Bates and Hervouet, 1998). Although this approach is more precise than others, it has been used only for some idealized estuarine cases because grid regenerations are necessary and therefore time-consuming in terms of computation. In the wet-dry point treatment method, the computational domain covers the entire basin of interest including intertidal area. The moving boundary between the land and sea, where water flux equals zero, is determined for each time step by the wet-dry point treatment technique. The wet and dry points are defined using the local total depth: when the depth is positive, it is defined as a wet point; otherwise it is a dry point. This method has been widely used in the depth-averaged 2D numerical models for estuaries including intertidal areas (Leendertse, 1970, 1987; Flather and Heaps, 1975; Leclerc *et al.*, 1990 Cheng *et al.*, 1993; Luettich, and Westerink, 1995a, 1995b, 1995c; Hubbert and McInnes, 1998; Ip *et al.*, 1998; Part *et al.*, 2002; Davis and Sheng, 2003). Applying the wet-dry point technique to 3D primitive equation models requires that the equations satisfy a finite value solution when the total depth approaches zero. In the z-coordinate system, the method used in the 2D model can be applied easily to the 3D case without any technical difficulties (Casulli and Cheng, 1991; Casulli and Cattani, 1994; Hervouet and Janin, 1994; Lin and Falconer, 1997; Gross *et al.*, 1999). However, to ensure numerical stability, the thickness of the layer closest to the surface must be greater than the amplitude of the tidal oscillation (Davies *et al.*, 1997; Lin and Falconer, 1997) as shown in Figure 1 (a). This constraint results in simulations difficult to use the wet-dry point method in an extremely shallow estuary like San Francisco Bay where the median depth is about 2m whereas the maximum tidal elevation reaches about 2.5m since it is impossible to include the vertical hydrodynamic structure that is frequently essential to predict the bed shear stresses and baroclinic motion on shallow basins in stratified estuaries.

The σ-transformation has been broadly used in coastal ocean models because it is well-suited for varying bottom topography as indicated in Figure 1 (b) (Blumberg and Mellor, 1983, 1987; Hedivogal *et al.*, 1991; Shchepetkin and McWilliams, 1998, 2003). This transformation is no longer valid if the total depth becomes zero. It seems hard to incorporate a wet-dry point treatment program in the σ-transformation model because of this limitation. Two methods have been

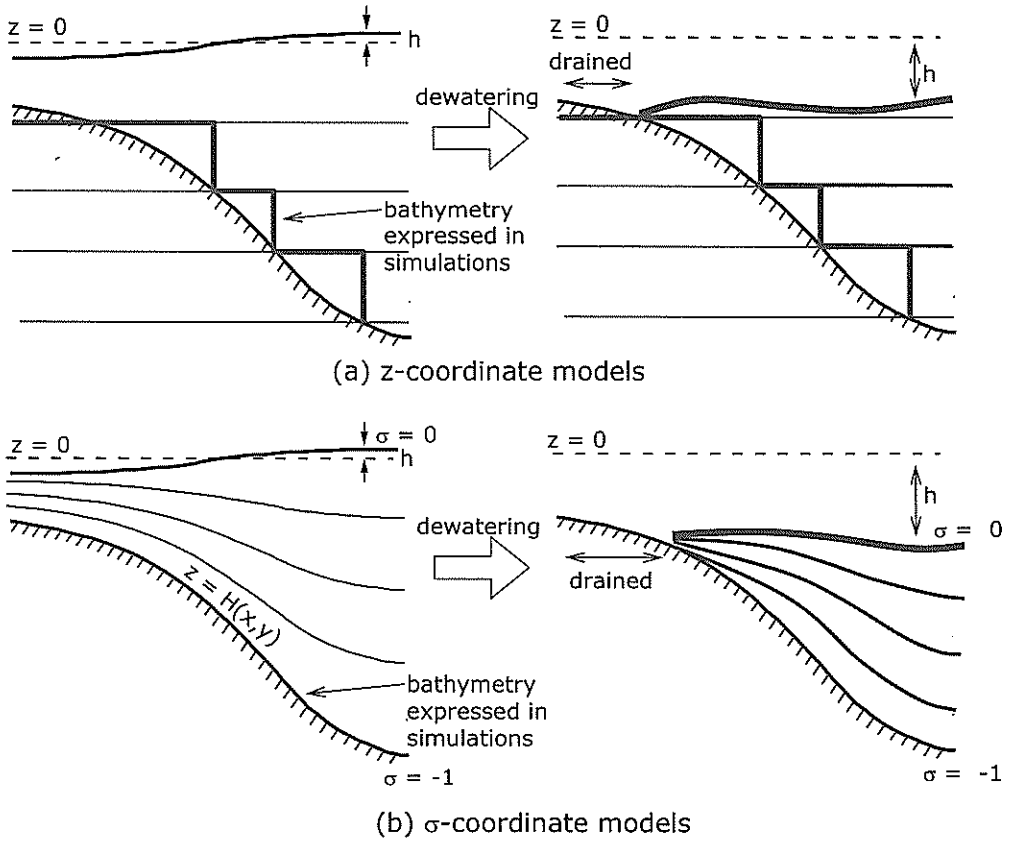

Figure 1: Schematic diagram of wetting and drying processes expressed by (a) z-coordinate models employed by Lin and Falconer (1997) and (b) σ-coordinate models by Xie *et al.* (2003).

proposed to avoid the occurrence of singular points when the local water depth approaches zero in the area of dry points. The first one assumes that the currents vanish at dry points as a result of infinite horizontal and vertical diffusion (Xie *et al.*, 2003). This approach is simple but it basically does not guarantee the volume conservation. The second method introduces an additional bottom boundary layer and redefines the local water depth as a sum of the real depth and the thickness of the bottom boundary layer as proposed by Ip *et al.* (1998) and Zheng *et al.* (2003; ZH03, hereafter). The second method seems accurate in mass conservation as compared to the first method. ZH03 explains that this additional thin layer, ranging from 1cm to 25cm, could be considered as a viscous sub-layer (ZH03) or porous media (Ip *et al.*, 1998) that lays beneath the logarithmic layer in turbulent boundary layer. However in the formulation of ZH03 as well as the model proposed by Ji *et al.* (2001), Xie *et al.* (2003) and Oey (2004), which are based on POM, ECOM (Blumberg *et al.*, 1993) and EFDC (Hamrick, 1992), they are considered to contain problems in the treatment of representing the bed boundary condition, since $\sigma = -1$ is defined at the bed surface, based upon the conventional logarithmic law of the wall. For instance, suppose the total depth becomes 10cm and 10 vertical σ layers are used in POM simulations which employ the Arakawa-C grid with uniform grid spacing, then the height of the horizontal velocities at the lowest grid point becomes 0.5cm above the bed while the typical value for the bed roughness height in estuaries may usually be 1.0cm. This means that the velocities closest to the bed are defined below the roughness height, and consequently the logarithmic law above the bed is no longer valid. It is thus required to develop a new methodology for reproducing bottom boundary layer precisely in extremely shallow estuaries and intertidal areas.

In the present study, a wetting and drying scheme (WDS) based on the wet-dry point method is developed to incorporate into a three-dimensional σ-coordinate

ocean model to simulate hydrodynamics in estuaries including intertidal areas such as mudflats and salt marshes (WD-POM). Attentions are paid particularly to the mass conservation and hydrodynamic processes near the bed by adapting an extended logarithmic law so as to precisely predict vertical profiles of currents in extremely shallow seas. WD-POM is at first applied to a run-up problem of non-linear long-waves on a sloping beach and is compared to the analytical solution proposed by Carrier and Greenspan (1958). Next the model is used to calculate tidal currents in San Francisco Bay, California, USA, which has large intertidal areas of about 200km^2 while the total surface area is 1240km^2. The accuracy of WD-POM is then confirmed with the harmonic analysis of the measured and the model-generated tidal elevations and currents. In addition, because the influence of intertidal bathymetry on estuarine hydrodynamics is of primary interest, the model is subsequently applied to simulate tidal waves and currents in San Francisco Bay. The model-generated result with WDS is compared with the result without WDS in order to exhibit the intertidal topographic effects on hydrodynamics in the bay.

2. METHODS

2.1 Brief description of Princeton Ocean Model

Princeton Ocean Model (POM) is based on a set of primitive equations consisting of the continuity equation, the 3D Reynolds-averaged Navier-Stokes equations, the heat and salinity transport equations, Mellor-Yamada level 2.5 turbulence closure model (Mellor and Yamada, 1982; Galperin *et al.*, 1988) for vertical eddy motion, and the Smagorinsky-type formulation for horizontal eddy viscosity and diffusivity with the Boussinesq approximation and the hydrostatic assumption. The governing equations are transformed from the 3D Cartesian coordinate into the 2DH orthogonal curvilinear coordinate and the vertical σ coordinate to smoothly resolve complex terrestrial geometries and marine bathymetries. The mode-split technique is used in POM to solve the governing equations, comprising the external mode to compute fast-moving 2DH surface gravity waves and the internal mode to estimate 3D vertical structure of currents, heat, salinity and turbulence. Several other techniques are also used to conserve numerical accuracy and to shorten computational times but they are not essential to the present study (for the detail, see Blumberg and Mellor, 1983, 1987).

2.2 Wetting and drying scheme

WD-POM is configured for a pre-defined computational domain that contains both wet and dry grid cells. A land mask function (LMF) is created to mask out all land cells during model simulations. The LMF is assigned zero for all land cells and unity for all water cells. The value of LMF at each grid cell is re-evaluated at each external time step based on a set of wetting-drying criteria. In the wetting and drying calculation presented here, the first step is to define three sub-depth scales, d_{cr}, d_{min}, and δ, prior to the simulations (Figure 2):

$$d_{cr} > d_{min} \geqq \delta \geqq 0. \tag{1}$$

The second step is to scan the total water depth at each grid cell, $D_{i,j} = H_{i,j} + \eta_{i,j}$, where $H_{i,j}$ is a vertical elevation in the z-coordinate below MSL (mean sea level) and $\eta_{i,j}$ is a water elevation above MSL in the z-coordinate at a certain external time step at a horizontal girid cell (i, j). If $D_{i,j} \leq d_{cr}$, the grid cell is regarded as potentially dry and WDS is immediately applied. In WDS three conditions are introduced to evaluate each of the potentially dry cells to be wet or dry by examining the four adjacent grid cells with;

a) min $[\eta_{i-1,j}, \eta_{i+1,j}, \eta_{i,j-1}, \eta_{i,j+1}] \leq \eta_{i,j}$,
b) min $[D_{i-1,j}, D_{i+1,j}, D_{i,j-1}, D_{i,j+1}] \leq d_{cr}$, or
c) max $[LMF_{i-1,j}, LMF_{i+1,j}, LMF_{i,j-1}, LMF_{i,j+1}] = 0$.

If at least one of these three conditions is satisfied, the potentially dry grid is considered effectively dry and is subsequently removed from the computational domain; the LMF is set to be 0. Otherwise the grid cell is considered wet and remains in the computational domain to be scanned again at the next time step; the LMF is held 1. When the cell becomes effectively dry, the water elevation $\eta_{i,j}$ is stored in the computer memory and restored in the next flooding. This procedure allows conserving the total water volume in the whole computa-

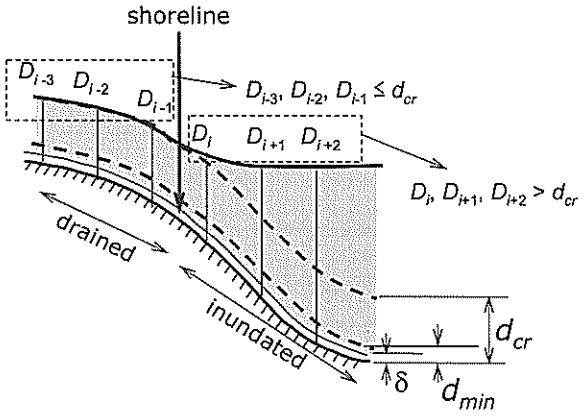

Figure 2: Conceptual illustration of the wetting and drying scheme presented here for a two dimensional vertical case. Onshore cells i-3 and i-2 are effectively dry and the cell i-1 is potentially dry. The condition a) is satisfied at the cell i-1 to be effectively dry while the cell i is still wet. Hence the shoreline (interface between a wet cell and a dry cell) can be defined between the cell i-1 and i.

tional domain during the simulations. WDS requires only flux-blocking conditions across the land-sea interfaces when wet cells become dry, while dry cells are temporarily dormant and are dynamically activated through the mass and momentum conservation.

The minimum depth, d_{min}, is used to avoid the zero depth because the σ-transformed primitive equations do not accept zero or negative water depths. When the horizontal grid spacing is sparse or the time step is set relatively large, the water surface may rapidly descend and be on or below the seabed during an external time step. In WD-POM, if the water depth $D_{i,j}$ at a potentially dry cell is rapidly dewatered and becomes less than d_{min} during one single time step, the cell is considered effectively dry, the local water depth is held d_{min}, and LMF is set zero. Whereas WDS itself is designed to conserve the water mass in the whole computational domain, it may no longer be valid if one employs no-zero d_{min}. However, the simulations become markedly robust with no-zero d_{min} if an external time step is set longer or very sparse horizontal grid spacing is configured. Introducing d_{min} is likely equivalent to defining a thin sub-layer on the bed as used in ZH03. The present method is more flexible since users can control the performance of WD-POM by adjusting the value of d_{min}. An example how WDS works in a 2D vertical case is conceptually illustrated also in Figure 2.

2.3 Extended logarithmic law for bed boundary layer representation

The last sub-depth scale in Eqn. (1), δ, is the most important one since it is used to retain the logarithmic velocity profile near the bed even though the total depth approaches zero. In other words, δ is necessary to reflect the vertical profiles within and above the bottom boundary layer and is indispensable to correctly estimate the bed shear stresses. In the original version of POM as well as the other versions used in the previous works by ZH03, Xie *et al.* (2003) and Oey (2004), the boundary condition for the horizontal components of 3D currents at the seabed is expresses as:

$$\frac{K_M}{D}\left(\frac{\partial U}{\partial \sigma},\ \frac{\partial V}{\partial \sigma}\right) = C_d\left[U^2+V^2\right]^{1/2}(U,\ V),\quad \sigma \to -1 \tag{2}$$

$$C_d = MAX\left[\frac{\kappa^2}{\left[\ln\{(1+\sigma_{kb-1})H/z_0\}\right]^2},\ 0.0025\right] \tag{3}$$

where K_M is vertical eddy diffusivity, U and V are the horizontal two components of the 3D velocities, C_d is a bed friction coefficient, κ is the von Karman constant, σ_{kb-1} is the lowest σ level for the horizontal current velocities, and z_0 is the roughness height usually being 1cm in estuaries. In the intertidal areas, variations in the water surface elevation η may be comparable to or greater than the water depth H relative to MSL, so that D should be used instead of H in Eqn. (3). In simulations of estuarine tidal currents, grid spacing may usually be exponentially decreased downwards resolve the bed boundary layer; the value of −0.991 for σ_{kb-1} is employed in the San Francisco Bay simulations described later. The profile of C_d according to the variable depth can be represented by the dotted curve in Figure 3 (a). The value of C_d is held constant to be 0.0025 if the total depth D is less than several hundred meters since POM is originally designed to simulate hydrodynamics in the ocean. This expression is considered to be undesirable for the boundary condition at the seabed in the intertidal com-

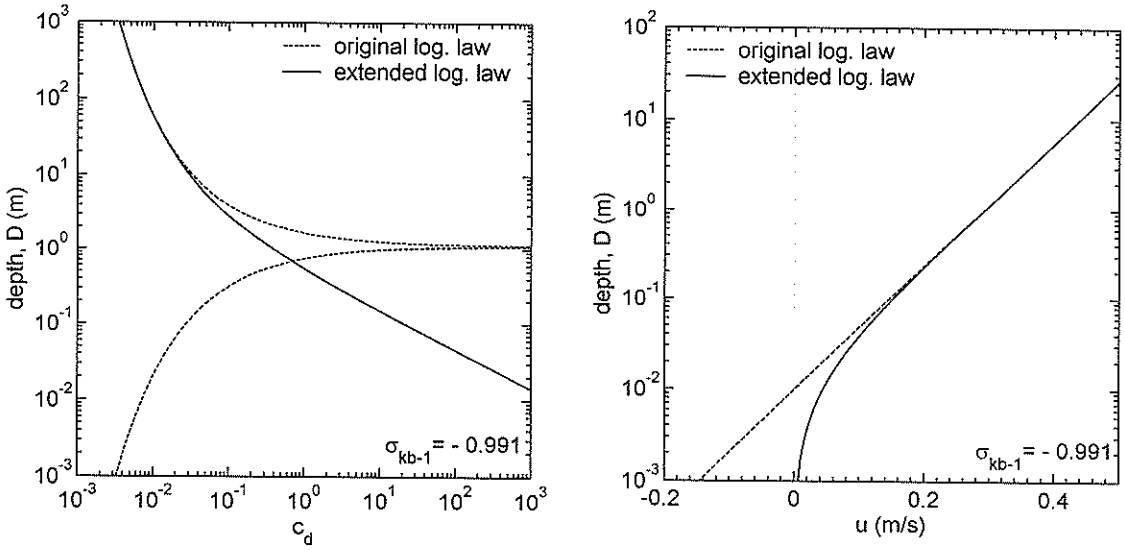

(a) vertical profiles of C_d (b) Velocity profiles on a logarithmic axis

Figure 3: Schematic diagrams of the original (dotted lines) and extended logarithmic (solid lines) profiles near the bed.

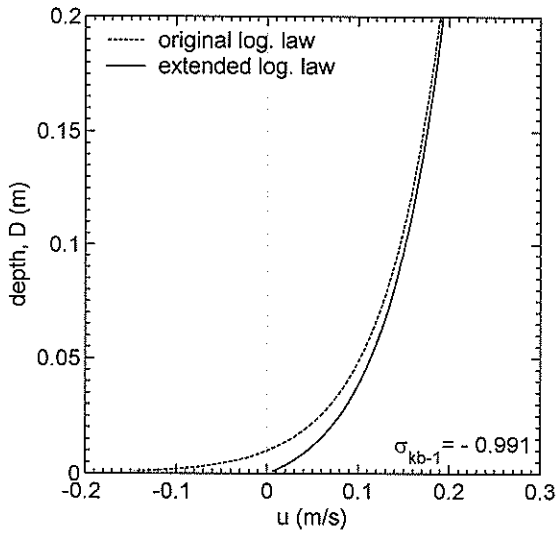

(c) Velocity profiles on a Cartesian axis

Figure 3: Continued.

putations. Therefore an extended logarithmic law represented by Eqn. (4) is introduced to reproduce the bottom boundary layer properly.

$$C_d = \frac{\kappa^2}{\left[\ln\left\{(1+\sigma_{kb-1})D/z_0 + \delta/z_0\right\}\right]^2} \tag{4}$$

Equation (4) introduces δ/z_0 in the denominator to avoid the logarithm in Eqn. (3) to be zero or negative (C_d thus becomes infinity) if the total depth is lowered to be extremely shallow. This procedure is explained technically to correspond to elevating the grid system vertically at δ as displayed in Figure 4. In hydrodynamics no discrepancy is expected because the bed shear stress used in the bottom boundary condition in POM is evaluated between the bed and the lowest grid points defined at $z = (1+\sigma_{kb-1})D/ z_0+\delta/z_0$. In practice the smaller value of δ is set, the more accurate estimation of the bed shear stresses can be achieved; the smallest value of $\delta = z_0$ is favorable as expressed in Eqn. (5).

$$C_d = \frac{\kappa^2}{\left[\ln\left\{(1+\sigma_{kb-1})D/z_0 + 1\right\}\right]^2} \tag{5}$$

Together with Eqn. (5), leaving the determination of l unchanged, where l is turbulent macroscale, the vertical eddy viscosity K_M and diffusivities K_H and K_q must be slightly altered to close the TKE and macroscale equations so that:

$$\left.\begin{aligned} K_M &= S_M q(l+\kappa\delta) = S_M q(l+\kappa z_0) \\ K_H &= S_H q(l+\kappa\delta) = S_H q(l+\kappa z_0) \\ K_q &= S_q q(l+\kappa\delta) = S_q q(l+\kappa z_0) \end{aligned}\right\}, \tag{6}$$

where S_M, S_H, S_q and are the stability functions and q is square root of TKE multiplied by 2, used in the Mellor-

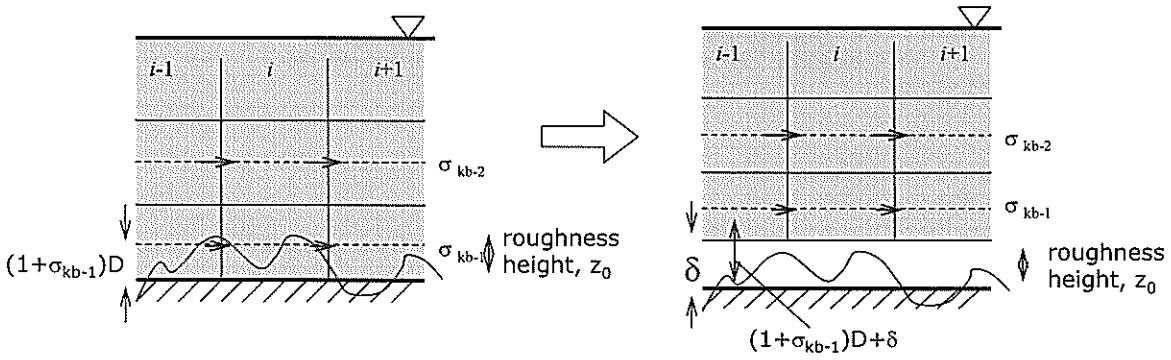

Figure 4: Definition sketch of δ. In the extended logarithmic law, the grid system is moved upwards at a height of δ.

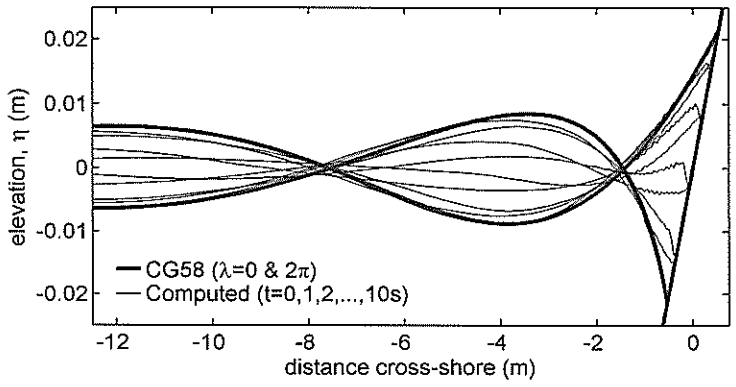

(a) Superposition of the instantaneous water-surface profiles

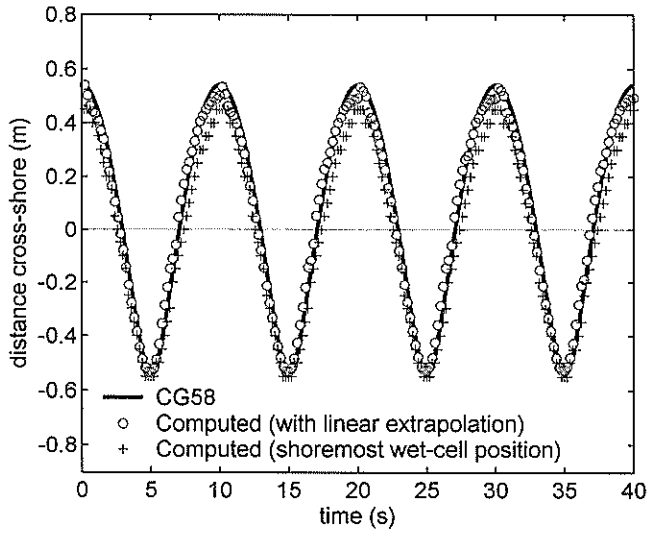

(b) Temporal variation of the computed shoreline positions

Figure 5: Comparison of the results from WD-POM and CG58.

Yamada level 2.5 sub-model in POM. The final result seems similar to that in the 1D model for the oscillatory boundary layer simulations by Mellor (2002). As illustrated in Figure 3 (b), the structure of the bottom boundary layer (vertical profiles of the horizontal current velocities) based on the original logarithmic law is much

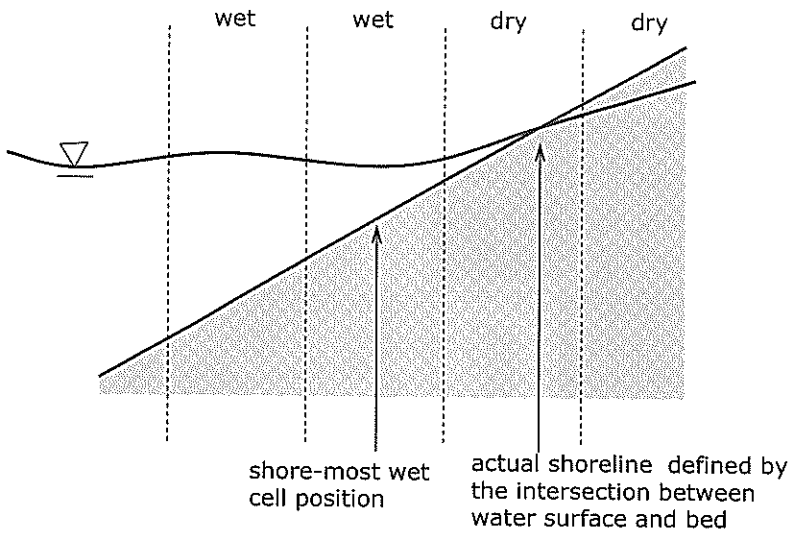

Figure 6: Definition of the shoreline position in Figure 5 (b) in a vertical 2D case. The model-predicted shore-most wet cell positions are converted with the linear extrapolation to estimate the actual shoreline positions as an interface between the wet and dry cells.

different from that based on the extended logarithmic law if $\delta = z_0$ is employed and $(1+\sigma_{kb-1})D/z_0+\delta/z_0$ approaches z_0. The velocity profiles estimated with the original logarithmic law shows that return flow is generated below z_0 as shown in Figure 3. The extended logarithmic law yields a little departure in its velocity profiles from that estimated by the original one when the depth decreases. Note that the extended logarithmic law is consistent with hydrodynamics near the seabed because the velocity profile estimated with the extended one coincides with that calculated with the original one if the profile with the extended one is moved upwards at a height of z_0 as indicated in Figure 3 (c). This means that the procedure expressed by Eqns. (5) and (6) is consistent with uplifting the grid system at a height of z_0. In addition, because δ is not used in the σ-transformation, δ is independent of D and can be set at zero if the simulations do not include the intertidal inundation and drainage.

3. RESULTS

3.1 Comparison to the analytical solution

Whereas WDS proposed here is formulated simplistically, it guarantees the water mass conservation and can control the numerical robustness in accordance with the value of d_{min}. WDS is modeled to precisely reproduce the benthic boundary layer if the computations are carried out for estuaries that have extremely shallow and/or intertidal areas. The numerical solutions derived from WD-POM are next compared to the analytical solution for swashing nonlinear long-waves on a linearly sloping beach (Carrier and Greenspan, 1958; CG58 hereafter). In the simulation, d_{cr}=1mm, d_{min}=0 and δ=0 are respectively employed for the three sub-depth scales, and the bed friction is thus neglected in the WD-POM simulation as is in CG58. Figure 5 (a) indicates superposition of water surfaces at several phases reproduced by the model and at the phases of 0 and 2π by CG58. The model-generated water surface seems to have a reasonable agreement with that calculated on the basis of CG58 although minor noises, which may be caused by reflected waves from the moving boundary, are produced near the shoreline, suggesting that WD-POM is capable of simulating the wetting and drying process in a laboratory scale. The temporal variations in the shoreline positions calculated by the model and CG58 are shown in Figure 5 (b). Although the model-generated shoreline is defined at the center of shore-most wet cells displayed with "plus" marks, manipulation should be done to estimate the actual shoreline defined at the intersection be-

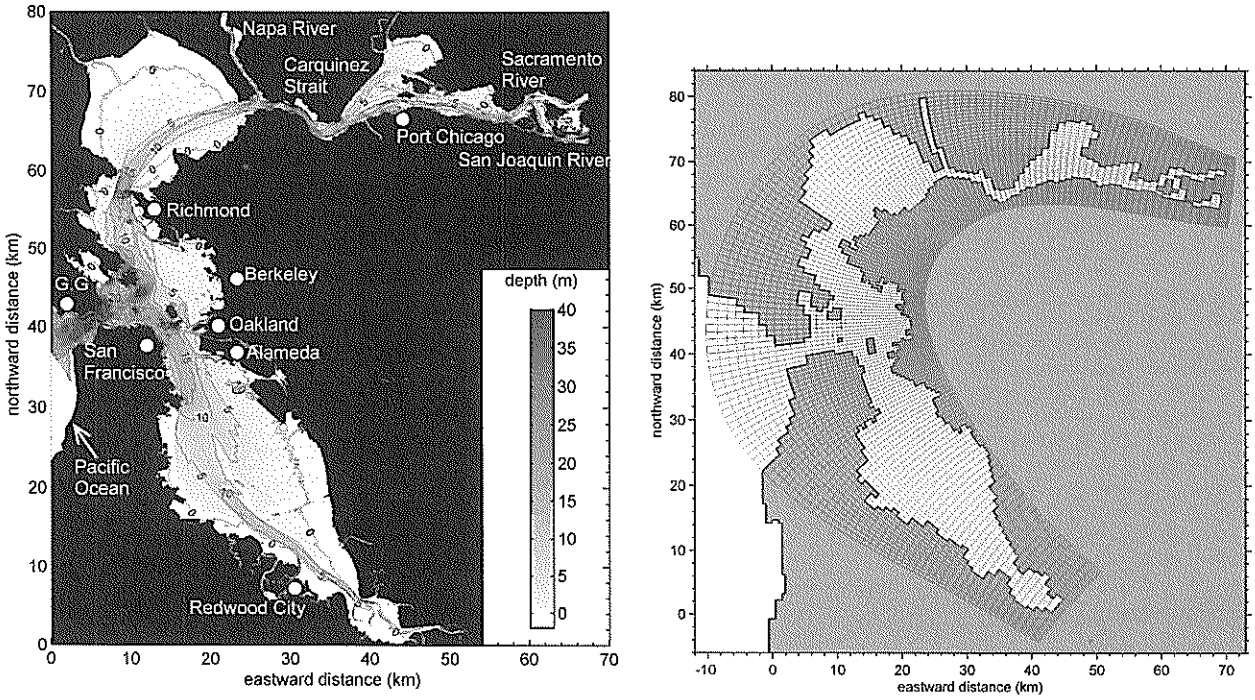

Figure 7: The bathymetric map of San Francisco Bay, California, USA (left) and the computational grid alignment using the horizontal orthogonal curvilinear transformation (right). The caption "G.G." shows Golden Gate. The bathymetry is relative to the MLLW level at San Francisco tide observatory (NOS-NOAA, 2003).

tween the water surface and the beach face as schematically illustrated in Figure 6. Shoreline positions calculated with the linear extrapolation are also indicated with circle marks in Figure 5 (b). The model-predicted shoreline movement reasonably agrees with the theory.

3.2 Tidal simulation in San Francisco Bay

The model is next applied to simulate tidal currents in San Francisco Bay, California, U.S.A. (Figure 7). The bay has the surface area of about 1240km^2 and is encompassed by intertidal mudflats of about 200km^2. South Bay, the southernmost part of San Francisco Bay, is often described as "a tidally oscillating lagoon with density-driven exchanges with the northern reach", and North Bay including San Pablo Bay and Suisun Bay has huge influx from the Sacramento-San Joaquin drainage basin (Conomos *et al.*, 1985). The simulation is performed for a total of 40 days including the first 3 days for the simulation spin-up (Cheng *et al.*, 1993) by solely imposing the astronomical tidal elevations on the open boundary situated off Golden Gate (the bay mouth). The density is held constant during the simulation and no fluvial freshwater fluxes nor wind forcing are considered. Ten vertical sigma layers, in which the downward grid spacing decreases exponentially, are assigned whilst 45 × 160 horizontal curvilinear cells are used in the simulation. The time steps for the external mode and the internal mode are set at 5s and 50s. The three sub-depth scales are set as d_{cr}=20cm, d_{min}= 5cm, and δ= z_0= 1cm, respectively.

The model-generated surface water elevations and 3D horizontal velocities in the whole computational domain are decomposed into the 17 dominant harmonic constituents and compared to the observed data as listed in Tables 1 and 2. The model result is verified to successfully reproduce propagation of the tidal waves and variations in the tidal currents observed in San Francisco Bay by NOAA-NOS (2003). Mass conservation check is next conducted as represented in Figures 8 and 9. The volume influx at the open boundary is almost equal to the volumetric change integrated for the whole computational domain, indicating that the volume is basically conserved except during the spring tide. Although some spiky but minor errors are found during this period,

Table 1: Four dominant components in the harmonic constituents of the tidal elevations (OBS: observed, MDL: model-predicted, DIF: difference between OBS and MDL)

		Amplitude (cm)			Phase (°)		
		OBS	MDL	DIF	OBS	MDL	DIF
M_2	Pt. Reyes	54.7	55.4	0.7	190.5	191.8	1.3
	San Francisco	58.1	57.8	−0.3	208.0	196.0	−12.0
	Alameda	68.6	66.3	−2.3	222.9	214.5	−8.4
	Redwood City	89.3	82.9	−6.4	238.0	233.4	−4.6
	Richmond	61.8	59.0	−2.8	222.1	216.2	−5.9
	Port Chicago	51.4	49.2	−2.2	283.4	299.0	15.6
S_2	Pt. Reyes	16.8	16.6	−0.2	188.4	188.5	0.1
	San Francisco	17.2	17.2	0.0	206.6	193.5	−13.1
	Alameda	19.6	18.8	−0.8	223.4	215.2	−8.2
	Redwood City	24.8	23.1	−1.7	243.0	239.8	−3.2
	Richmond	17.4	16.8	−0.6	223.0	214.9	−8.1
	Port Chicago	14.1	12.3	−1.8	283.1	301.1	18.0
K_1	Pt. Reyes	32.6	32.5	−0.1	207.7	208.2	0.5
	San Francisco	32.0	32.8	0.8	211.5	209.4	−2.1
	Alameda	32.7	33.7	1.0	217.8	217.9	0.1
	Redwood City	35.3	35.4	0.1	224.5	228.8	4.3
	Richmond	32.1	32.5	0.4	218.4	220.0	1.6
	Port Chicago	27.0	28.6	1.6	255.3	268.7	13.4
O_1	Pt. Reyes	24.0	24.2	0.2	203.9	203.9	0.0
	San Francisco	23.8	24.6	0.8	207.4	204.4	−3.0
	Alameda	23.7	24.5	0.8	212,9	211.2	−1.7
	Redwood City	24.3	24.0	−0.3	219.3	219.8	0.5
	Richmond	23.3	23.9	0.6	213.4	213.1	−0.3
	Port Chicago	18.3	19.3	1.0	245.8	256.5	11.3

Table 2: Four dominant components in the harmonic constituents of the tidal currents (OBS: observed, MDL: model-predicted, DIF: difference between OBS and MDL)

		Major Axis (cm/s)			Orientation (°)			Phase Epoch (°)		
Locations		OBS	MDL	DIF	OBS	MDL	DIF	OBS	MDL	DIF
Richmond	M_2	75.8	68.6	−7.2	118.8	105.2	−13.6	176.4	170.8	−5.6
	S_2	21.6	19.3	−2.3	116.0	105.4	−10.6	172.8	168.1	−4.7
	K_1	23.3	21.7	−1.6	121.6	105.5	−16.1	161.8	157.9	−3.9
	O_1	16.7	14.0	−2.7	120.2	105.4	−14.8	155.0	148.7	−6.3
Oakland	M_2	52.5	48.6	−3.9	99.8	103.7	3.9	326.6	325.6	1.0
	S_2	14.6	16.7	1.9	102.0	103.4	1.4	318.1	318.2	0.1
	K_1	10.4	11.8	1.4	100.0	105.1	5.1	298.6	309.7	11.1
	O_1	4.5	6.0	1.5	110.7	106.8	−3.9	277.2	297.2	20.0

it returns to have a value of about zero (i.e., no error is measured) immediately after the spring tide.

Instantaneous distributions of 2DH current vectors, water surface elevations, and dry cells at two phases during the spring tide, at ebbing and high slack phases, are displayed in Figure 10. The current fields are realistic and agree with the results by Cheng *et al.* (1993); the water surface rises and descends to inundate and drain out intertidal areas formed on the fringe of the bay and the currents are strong along the deeper channel while weak on the shallow areas.

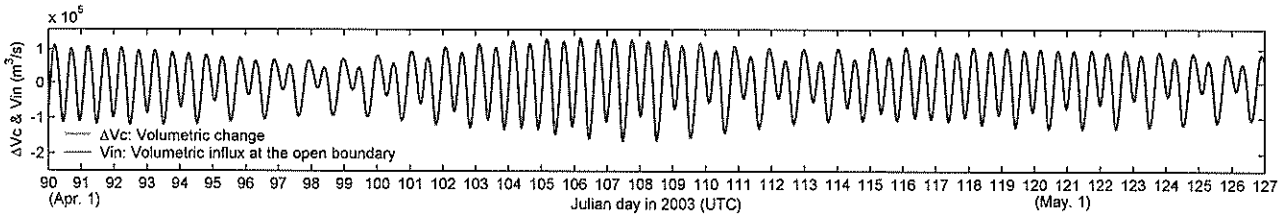

Figure 8: Volume influx at the open boundary, V_{in}, and volumetric change, ΔV_c.

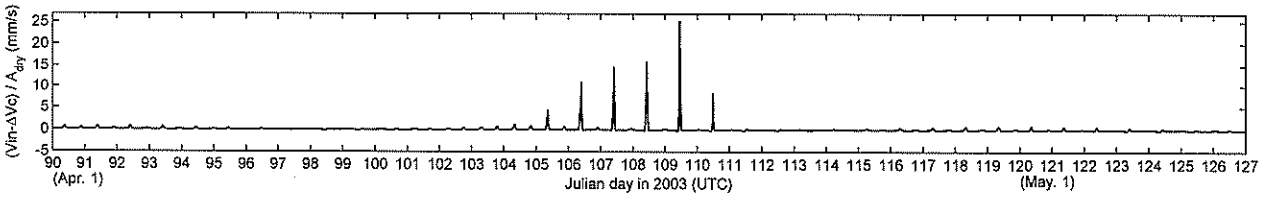

Figure 9: Errors in volume flux per unit area of dry cells, $(V_{in}-\Delta V_c)/A_{dry}$: A_{dry} is drained area.

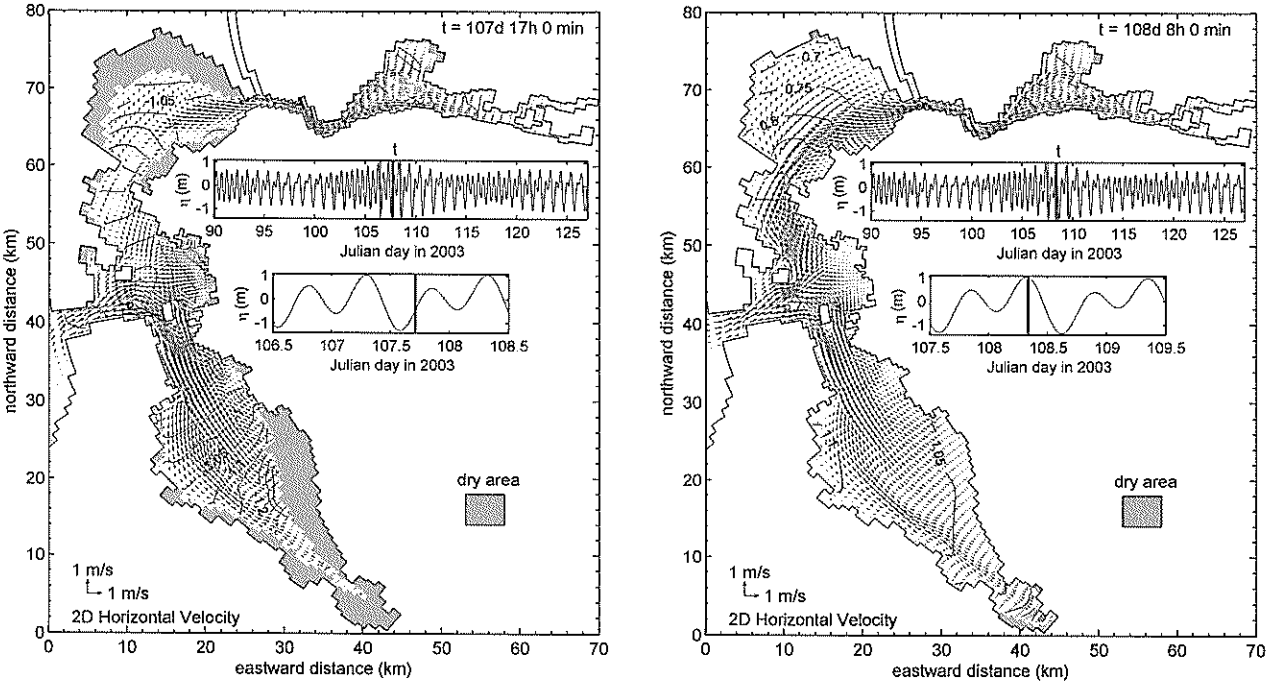

Figure 10: Distributions of the model-generated 2DH current velocities, water elevations, and dry cells at an ebbing phase (left) and at a high slack phase (right) during the spring tide.

4 DISCUSSION

Effects of intertidal topography on estuarine hydrodynamics are of interest. Two computations are thus carried out in order to examine a role of shallow fringes. One computation is done with the actual bathymetry of San Francisco Bay shown in Figure 7, whereas the other uses a modified bathymetry in which the depths in the shallow areas less than 2m deep are replace by the depth of 2m (i.e., $H \geq 2$m). In other words, the first one takes account of WDS (Case 1: w/ WDS, hereafter), and the latter does not consider WDS (Case 2: w/o WDS). To simplify comparison of tidally-averaged features between the two simulations, only a monochromatic sinusoidal tidal wave at a period of 12 h with amplitude of

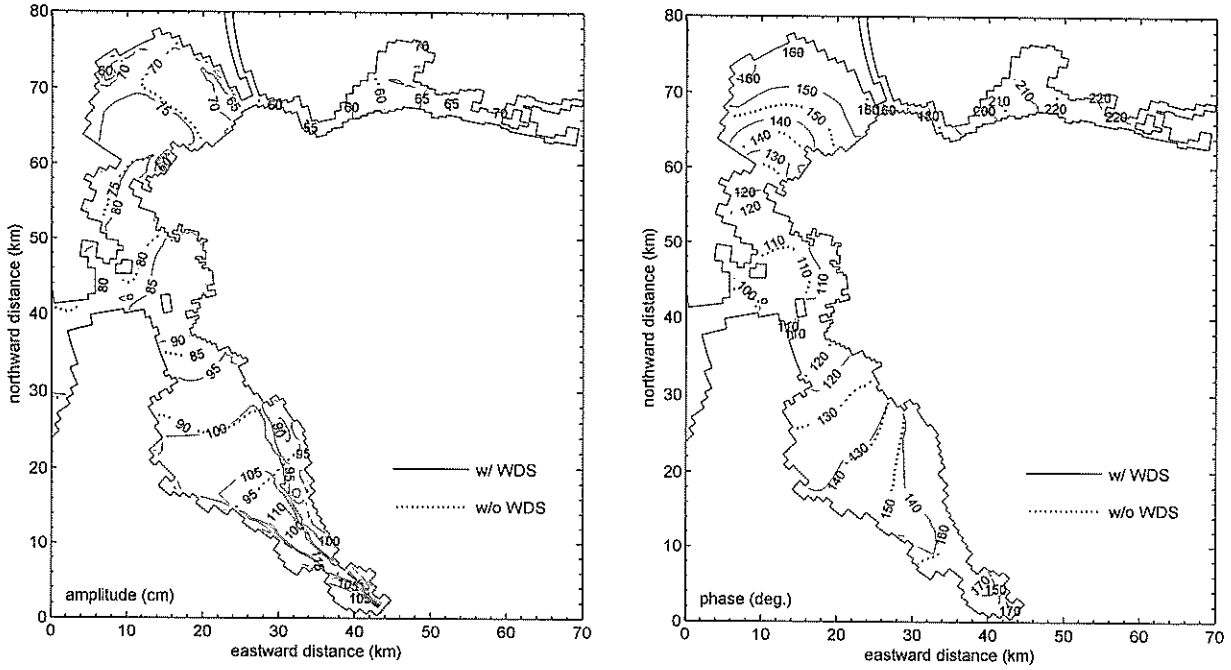

Figure 11: (Left) iso-tidal amplitude and (right) iso-phase charts estimated with the harmonic analysis for the simulated results w/ WDS (Case 1) and w/o WDS (Case 2).

0.8m is imposed at the open boundary off Golden Gate. This tidal wave approximately coincides with the M_2 tide which is the predominant tidal component in San Francisco Bay (Conomos *et al.*, 1985). Simulated water elevations are decomposed with the harmonic analysis to estimate co-tidal amplitude and co-phase charts as displayed in Figure 11. The both panels in Figure 11 exhibit significant difference between two cases can be found particularly in the southern and northern reaches of the bay remote from the bay mouth; the tidal amplitudes calculated in Case 1 (w/ WDS) are 5 to 10cm larger than those in Case 2 (w/o WDS), while the phases are slightly delayed at 5 to 20 degrees (i.e., 10 to 40 minutes) in Case 1 behind those in Case 2.

In San Pablo Bay located in the southwest part of San Francisco Bay, the tidal waves are propagating anticlockwise as Kelvin waves attenuated by bottom-frictional drag as presented by Hendershott and Speranza (1971). In the present simulations, possible processes would be refraction and shoaling of the tidal waves due to the sloping bathymetry in the shallow fringes, and centrifugal forces induced by horizontally curved geometry of the bay (Lacy and Monismith, 2001). Spatial distributions of tidal ellipses and tidal residual current vectors in San Pablo Bay calculated with the results of two computations seem to be similar in almost the whole domain as shown in Figure 12, but slightly different particularly in the shallow regions at the depth of less than 2m. The tidal currents near the shoreline in Case 2 (w/o WDS) show that the principal directions of the tidal ellipses are nearly parallel to the shore and that the tidal waves are progressive because the tidal ellipses are more circular. By contrast in Case 1 (w/ WDS), the tidal waves are traveling and being refracted on the shallow basins to generate the shore-normal components. The shapes of the tidal ellipses turn into more linear to demonstrate that oscillatory standing waves are predominant in Case 1. In addition, it is interpreted that the phase of the tidal waves in Case 1 significantly retards probably because of the bed friction on the shallows, while the tidal amplitude is amplified owing to the reflected waves on the shallow slopes to form partially standing waves. The resultant residual currents are also different in the shallow fringes; the residual vectors align normal to the isobaths in Case 1 (w/ WDS) whereas parallel to the shoreline in Case 2 (w/o WDS). As a result, a circulating current pattern in San Pablo Bay seems to be more attenuated in Case 1 (w/ WDS) than that in Case 2 (w/o

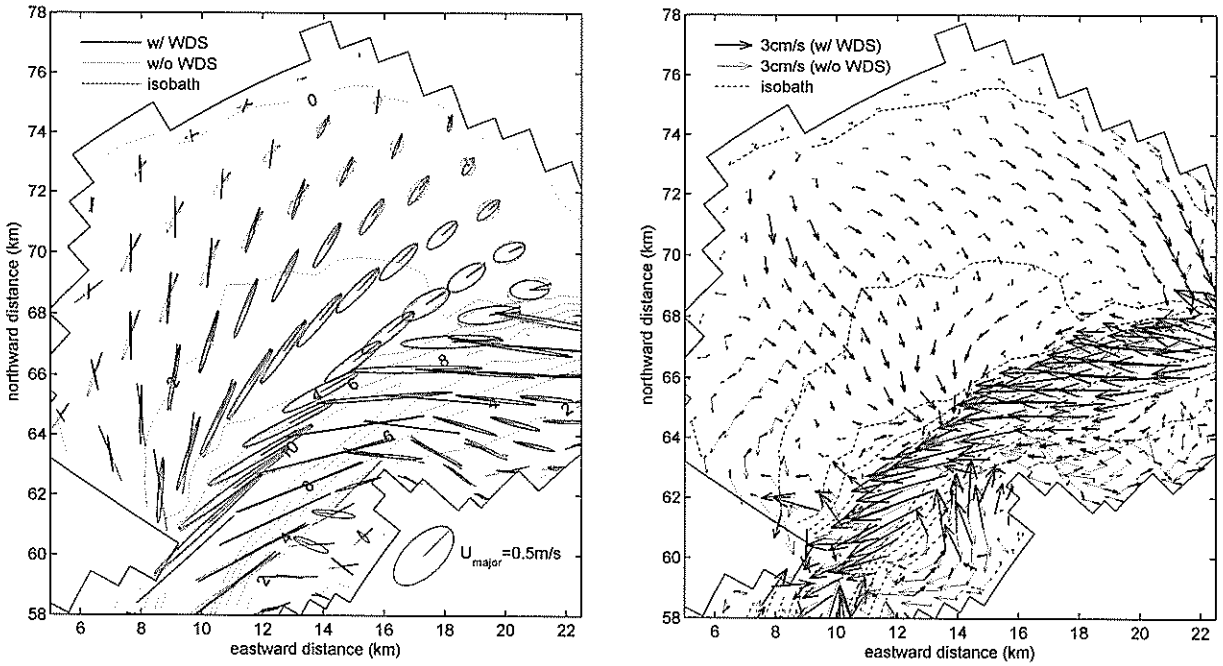

Figure 12: (Left) tidal ellipses and (Right) tidal residual current vectors based on the harmonic analysis with the result of Case 1 (w/ WDS) and Case 2 (w/o WDS).

WDS). These results suggest that the directions of the tidal residual fluxes can also be significantly different in response to the intertidal topographies.

5 CONCLUSIONS

A wetting and drying scheme for a three-dimensional terrain-following coastal ocean model (POM, Blumberg and Mellor, 1983, 1987) is developed with consideration of the mass conservation and computational robustness. An extended logarithmic law for the intertidal simulations is proposed to precisely reproduce the bed shear stresses and the velocity profiles within and above the bed boundary layer. The model results are verified by comparing to the analytical solution by Carrier and Greenspan (1958) theory and the observed data in San Francisco Bay, California, USA, by NOS- NOAA (2003) to show a reasonable agreement in the variations in water surface elevations, 3D current velocities, and shoreline positions.

Effects of the intertidal topography on estuarine hydrodynamics are examined by performing two simulations with and without the wetting and drying process. The intertidal topography is demonstrated to play a significant role in altering the propagation of the tidal waves and formation of the tidal residual currents. The tidal waves propagating as anticlockwise Kelvin waves are found to generate the shore-normal velocity component, and thus become partially standing waves, during flood onto the intertidal sloping bathymetry while the shore-parallel component is predominant in the tidal currents without the wetting and drying. The intertidal effects are also observed from the simulations so that the tidal amplitude is also enhanced on the intertidal areas because of shoaling of the tidal waves. The phases, in contrast, are visibly retarded as the bed frictional drag acts on the intertidal currents more on the intertidal areas.

(Accepted on August 10, 2004)

ACKNOWLEDGEMENTS

This research project was partially supported by Japan Society for Promotion of Science and is a part of the author's work during his stay at University of California, Berkeley, USA, since March 2002 till March 2004.

The author would like to express sincere appreciation to Professor Mark T. Stacey of UC Berkeley, and Professor Rodney J. Sobey of Imperial College of London, UK, for their helpful comments on the manuscript. Thanks are also due to Drs. Hirofumi Hinata and Keisuke Nakayama of National Institute for Land and Infrastructure Management, Japan, for their comments on the numerical modeling.

REFERENCES

Austria, P.M. and Aldama, A.A., 1990. Adaptive mesh scheme for free surface flows with moving boundaries, In Gambolati, G., Rinaldo, A., Brebbiam, C.A., Fray, W.G. and Pinder, G.F. (eds.), *Computational Methods in Surface Hydrology*, Springer-Verlag, New York, USA, 456-460.

Austen, I., Andersen, T.J. and Edelvang, K., 1999. The influence of benthic diatoms and invertebrates on the erodibility of an intertidal mudflat, the Danish Wadden Sea, *Estuarine, Coastal and Shelf Sci.*, 49: 99 – 111.

Bates, P.D. and Hervouet, J.-M., 1998. A new method for moving-boundary hydrodynamic problems in shallow water, *Proc. R. Soc. Lond. A*, 455, 3107-3128

Blumberg, A.F. and Mellor, G.L., 1983. Diagnostic and prognostic numerical circulation studies of the South Atlantic Bight, *J. Geophys. Res.*, 88: 4579-4593.

Blumberg, A.F. and Mellor, G.L., 1987. A description of a three-dimensional coastal ocean circulation model, In Three-dimensional Coastal Ocean Models, Vol.4, Heaps, N. (ed.), Ameri. Geophys. Union, Washington D.C., pp.208.

Blumberg, A.F., Signell, R.P. and Jenter, H.L., 1993. Modeling transport processes in the coastal ocean, *J. Mar. Envir. Eng.*, 1: 31-52.

Carrier, G.F. and Greenspan, H.P., 1958. Water waves of finite amplitude of a sloping beach, *J. Fluid Mech.*, 4: 97-109.

Casulli, V. and Cheng, R.T., 1991. A semi-implicit finite-difference model for three-dimensional tidal circulation, In Spaulding, M., Swanson, C., Cheng, R., Blumberg, A. and Bedford, K. (eds), *Proc. 2nd Intl. Conf. Estuarine and Coastal Modeling*, Ameri. Soc. Civil. Eng., Tampa, FL, USA, 620-631.

Casulli, V. and Cattani, E., 1994. Stability, accuracy and efficiency of a semi-implicit method for three-dimensional shallow water flow, *Computers and Mathematics with Application*, 27: 99-112.

Cheng, R.T., Casulli, V. and Gartner, J.W., 1993. Tidal, residual, intertidal mudflat (TRIM) model and its application to San Francisco Bay, California, *Estuarine, Coastal and Shelf Sci.*, 36: 235-280.

Conomos, T.J., Smith, R.E. and Gartner, J.W., 1985. Environmental setting of San Francisco Bay, *Hydrobiologia*, 129: 1-12.

Davies, A.M., Jones, J.E. and Xing, J., 1997. Review of recent developments in tidal hydrodynamic modeling, I: Spectral models, *J. Hydraulic Eng.*, 123, 278-292.

Davis, J.R. and Sheng, Y.P., 2003. Development of parallel storm surge model, *Int. J. Numerical Methods in Fluids*, 42: 549-580.

Flather, R.A. and Heaps., N.S., 1975. Tidal computations for Morecambe Bay, *Geophys. J. of the Royal Astronomical Society*, 42, 489-517.

Galperin, B., Kantha, L.H., Hassid, S. and Rosati, A., 1988. A quasi-equilibrium turbulent energy model for geophysical flows, *J. Atmos. Sci.*, 45: 55-62.

Gross, E.S., Koseff, J.R. and Monismith, S.G., 1999. Three-dimensional salinity simulations of South San Francisco Bay, *J. Hydraulic Eng.*, 125, 1199-1209.

Hamrick, J.M., 1992. *A three-dimensional environmental fluid dynamics computer code: theoritical and computational aspects*, Special Report 317, The College of William and Mary, Virginia Institute of Marine Science, Williamsburg, VA, 63p.

Haidvogel, D. B., Wilkin, J.L. and Young, R., 1991. A semi-spectral primitive equation ocean circulation model using vertical sigma and orthogonal curvilinear horizontal coordinates, *J. Comp. Phys.*, 94: 151-184.

Hendershott, M.C. and Speranza, A., 1971. Co-oscillating tides in long, narrow bays; the Taylor problem revisited, *Deep-Sea Res.*, Vol.18, pp.959-980.

Hervouet, J.M. and Janin, J.M., 1994. Finite-element algorithms for modeling flood propagation, In Molinaro, P. and Ntale, L. (eds.), *Modeling of Flood Propagation Over Initially Dry Areas*, Ameri. Soc. Civil. Eng., New York, NY, 102-113.

Hervouet, J.-M. & Van Haren, L. 1996. Recent advances in numerical methods for fluid flows, In: Anderson,

M.G., Walling, D.E. and Bates, P.D. (eds), *Floodplain processes*, Wiley, Chichester, UK, 183-214.

Hubbert, G.D. and McInnes, K.L., 1999. A storm surge model for coastal planning and impact studies, *J. Coastal Res.*, 15 (1), 168-185.

Ip, J.T.C., Lynch, D.R. and Friedrichs, C.T., 1998. Simulation of estuarine flooding and dewatering with application to Great Bay, New Hampshire, *Estuarine, Coastal and Shelf Sci.*, 47, 119-141.

Ji, Z-G., Morton, M.R. and Hamrick J.M., 2001. Wetting and drying simulation of estuarine processes, *Estuarine, Coastal and Shelf Sci.*, 53: 683-700.

Johns, B., Dube, S.K., Sinha, P.C., Mohanty, U.C. and Rao, A.D, 1982. The simulation of a continuously deforming lateral boundary in problems involving the shallow water equations, *Computer and Fluids*, 10, 105-116.

Kuwae, T., Hosokawa, Y., and Eguchi, N., 1998. Dissolved inorganic nitrogen cycling in Banzu intertidal sand-flat, Japan, *Mangroves and Salt Marshes*, 2: 167-175.

Lacy, J. and Monismith, S.G., 2001. Secondary currents in a curved, stratified channel, *J. Geophys. Res.*, 106 (C12): 31,283-31,302.

Leclerc, M., Bellemare, J-F., Dumas, G. and Dhatt, G., 1990. A finite element model of estuarian and river flows with moving boundaries, *Advances in Water Resources*, 13: 158-168.

Leendertse, J.J., 1970. A water-quality simulation model for well mixed estuaries and coastal seas: Principles of computation, *Report RM-6230-RC*, Vol. I, Rand Corporation, Santa Monica, CA.

Leendertse, J.J., 1987. Aspects of SIMSYS2D, a system for two-dimensional flow computation, *Report R-3572-USGS*, Rand Corporation, Santa Monica, CA.

Le Hir, P., Roberts, W., Cazaillet, O., Christie, M., Bassoullet, P. and Bacher, C., 2000. Characterization of intertidal flat hydrodynamics, *Continental Shelf Res.*, 20: 1433 – 1459.

Lin, B. and Falconer, R.A, 1997. Three-dimensional layer-integrated modeling of estuarine flows with flooding and drying, *Estuarine, Coastal and Shelf Sci.*, 44, 737-751.

Luettich, R.A. and Westerink, J.J, 1995a. An assessment of flooding and drying techniques for use in the ADCIRC hydrodynamic model: implementation and performance in one-dimensional flows, *Report for the Department of the Army*, DACW39-94-M-5869.

Luettich, R.A. and Westerink, J.J., 1995b. Implementation and testing of elemental flooding and drying in the ADCIRC hydrodynamic model, *Final Report for the Department of the Army*, DACW39-94-M-5869.

Luettich, R.A. and Westerink, J.J., 1995c. Continental shelf scale convergence studies with a barotropic tidal model, *Coastal Estuarine Stud.*, 47: 349-371.

Lynch, D.R. and Gray, W.G., 1980. Finite element simulation of flow in deforming regions, *J. Computational Physics*, 36, 135-153.

Mellor, G.L., 2002. Oscillatory Boundary Layers, *J. Phys. Oceanogr.*, 32: 3075-3088.

Mellor, G.L. and Yamada, T., 1982. Development of a turbulence closure model for geophysical fluid problems, *Rev. Geophys. Space Phys.*, 20: 851-875.

National Ocean Service, National Oceanic and Atmospheric Administration (NOS-NOAA), 2003. http://www. co-ops.nos.noaa.gov/.

Oey, L-Y., 2004. A wetting and drying scheme for POM, *Ocean Modeling*, 9. (in press)

Park, K., Oh, J.-H., Kim, H.-S. and Im, H.-H., 2002. Case study: Mass transport mechanism in Kyunggi Bay around Han River mouth, Korea, *J. Hydr. Eng.*, 128: 257-267.

Shchepetkin, A.F., McWilliams, J.C., 1998. Quasi-monotone advection schemes based on explicit locally adaptive dissipation. *Mon. Wea. Rev.* 126, 1541–1580.

Shchepetkin, A.F., McWilliams, J.C., 2003. The regional ocean modeling system: a split-explicit, free-surface, topography-following coordinate ocean model. *J. Geophys. Res.*, 108: 3501-3534.

Shi, F., 1995. On moving boundary numerical models of coastal sea dynamics, Ph.D. Dissertation, Ocean Univ. of Qingdao, Qingdao, China.

Siden, G.L.D. and Lynch, D.R., 1988. Wave equation hydrodynamics o n deforming elements, *Intl. J. Numerical Methods in Fluids*, 8, 1071-1093.

Talke, S.A. and Stacey, M.T., 2003. The influence of oceanic swell on flows over an estuarine intertidal mudflat in San Francisco Bay, *Estuarine, Coastal and Shelf Sci.*, 58: 541-554.

Uchiyama, Y., Kuriyama, Y. and Katoh, K., 2001. Suspended sediment and morphological response on Banzu tidal flat, Japan, *Proc.4th Int'l Conf. Coastal Dynamics*, Ameri. Soc. Civil Eng., Lund, Sweden: 1038-1047.

Van Der Lee, W.T.B., 2000. Temporal variation of floc size and settling velocity in the Dollard estuary, *Continental Shelf Res.*, 20: 1495 – 1511.

Whitehouse, R.J.S., Soulsby, R.L., Roberts, W. and Mitchener,H.J., 2000. Intertidal Processes, In: *Dynamics of estuarine muds*, Thomas Telford, London, UK: 163-168.

Xie, L., Pietrafesa, L.J. and Peng, M., 2003. Incorporation of a mass-conserving inundation scheme into a three dimensional storm surge model, *J. Coastal Res.*, 1-17.

Zheng, L., Chen, C. and Liu, H., 2003. A modeling study of the Satilla River Estuary, Georgia. I: Flooding-drying process and water exchange over the salt marsh-estuary-shelf complex, *Estuaries*, 26 (3): 651-669.

港湾空港技術研究所報告　第43号第4巻

２００４．１２

編集兼発行人　独立行政法人港湾空港技術研究所

発　行　所　独立行政法人港湾空港技術研究所
横須賀市長瀬３丁目１番１号
TEL. 046(844)5040　URL. http://www.pari.go.jp/

印　刷　所　昭和情報プロセス株式会社